Title

Coordination of membrane synthesis with cell growth: the *Escherichia coli* phospholipid synthesis enzyme PlsB responds to membrane abundance in a manner consistent with filamentation-mediated inhibition

Author List

Jaïrus Beije, Desi Fierlier, Margot Guurink, Amba Stapert, Adja Zoumaro-Djayoon, Gregory Bokinsky

Affiliations

Department of Bionanoscience, Kavli Institute of Nanoscience, Delft University of Technology, Delft, The Netherlands.

Materials and correspondence: g.e.bokinsky@tudelft.nl

Abstract

Cell viability demands tight coordination between growth and the synthesis of new membrane. The mechanisms coordinating cell growth with membrane synthesis in any organism are unclear. In *Escherichia coli,* initiation of phospholipid synthesis by the glycerol-3-phosphate acyltransferase PlsB is regulated by cell growth via an unknown allosteric mechanism. Previous studies have established that PlsB assembles into enzymatically inactive, membrane-bound filaments when overexpressed. We propose that PlsB filamentation regulates PlsB activity and coordinates membrane synthesis with growth. Here, we test our hypothesis by observing the localization of fluorescently labelled PlsB using live-cell fluorescence microscopy. During growth, PlsB localizes as discrete foci, consistent with formation of inactive filaments. Reducing cellular membrane content eliminates PlsB foci and delocalizes PlsB into the cytoplasm. Restoring membrane synthesis causes PlsB foci to reform after a delay. These results are consistent with our hypothesis and suggest a model in which PlsB reversibly assembles into inactive filaments in response to phospholipid abundance. This mechanism establishes a negative feedback loop that controls initiation of phospholipid synthesis by PlsB and effectively coordinates membrane synthesis with growth.

30 # Introduction

31 How do cells grow without breaking their membranes? Cells must tightly coordinate cell envelope
32 synthesis with growth to maintain viability. This ability is essential for all cells and yet is not
33 understood in any organism. The membrane synthesis pathway of the model prokaryote
34 *Escherichia coli* is perhaps the best-characterized to date (1). *E. coli* is a Gram-negative bacterial
35 species whose inner membrane is composed of phospholipids while the outer membrane is an
36 asymmetric bilayer featuring a phospholipid inner leaflet and a lipopolysaccharide outer leaflet. The
37 synthesis of membrane phospholipids is initiated in the cytoplasm by the peripheral membrane
38 enzyme PlsB, which transfers fatty acids from acyl thioesters to glycerol-3-phosphate (G3P) to
39 generate lysophosphatidic acid (LPA) (**Fig. 1A**). LPA is further acylated by PlsC to generate
40 phosphatidic acid (PA), the universal precursor of glycerophospholipids (2). Subsequent reactions
41 add headgroups to the G3P backbone, yielding membrane phospholipids phosphatidylglycerol (PG)
42 and phosphatidylethanolamine (PE). While LPA is also generated via PlsX and PlsY, this pathway is
43 not essential in *E. coli,* indicating that most LPA is synthesized by PlsB (3). Synthesized
44 phospholipids partition into the inner membrane and are subsequently transferred to the inner leaflet
45 of the outer membrane by several redundant protein bridges (4).

46 As the first enzyme of the phospholipid synthesis pathway, PlsB activity determines the rate
47 of membrane phospholipid synthesis. Thus, PlsB activity must be synchronized with growth.
48 Phospholipid synthesis flux during steady-state growth is not controlled by concentrations of PlsB
49 substrates (G3P and fatty acyl thioesters) or by PlsB concentration (5–8). Furthermore, PlsB
50 overexpression does not increase phospholipid abundance (9, 10). Thus, PlsB activity must be
51 regulated by an allosteric mechanism that activates and deactivates PlsB according to an allosteric
52 signal. Despite extensive biochemical studies, potential allosteric mechanisms controlling PlsB
53 activity have remained elusive (11–15). Intriguingly, an early study discovered that PlsB assembles
54 into protein filaments that are readily detectable if PlsB is overexpressed (10). PlsB filaments consist
55 of a repeating unit (likely PlsB dimers) helically arranged around a phospholipid core (16). While
56 filamentous PlsB is enzymatically inactive, dissolution of PlsB filaments with a mild detergent

57 restores activity. Whether filamentation coordinates PlsB activity with cell growth has remained
58 unexplored.

59 Recently, filamentation is increasingly appreciated as a mechanism for regulating metabolic
60 enzymes (17, 18). High-throughput imaging screens and biochemical experiments have found that
61 many metabolic enzymes reversibly assemble into filaments (19, 20). Often, filamentation and
62 inhibition are triggered by the accumulation of a product metabolite (21, 22). In these cases,
63 filamentation enables negative feedback control over enzyme activity in response to product
64 demand. Maintaining a fraction of the enzyme population in such an inactive form (described as
65 "excess capacity" or "enzyme storage") ensures that biosynthetic activity can be rapidly increased
66 when needed (23).

67 How might filamentation play a role in regulating PlsB? By analogy to other filament-forming
68 enzymes, PlsB might assemble into inactive filaments due to accumulation of excess membrane
69 phospholipids. The fraction of cellular PlsB that is sequestered into inactive filaments might vary in
70 proportion with the density of phospholipids within the inner membrane: a higher surface density of
71 phospholipids would tend to increase the fraction of PlsB within a filament, decreasing overall PlsB
72 activity, while decreased phospholipid content would liberate PlsB from filaments and increase the
73 active fraction (**Fig. 1B**). This mechanism would establish a direct link between membrane
74 phospholipid abundance and PlsB activity that acts as a classic negative feedback loop (**Fig. 1C**)
75 and coordinates phospholipid synthesis with growth (**Fig. 1D**). Intriguingly, *in vitro* experiments
76 suggest that excess phospholipids (generated by membrane compression) are extruded from
77 membranes as small lipid filaments (24). Such lipid filaments might nucleate the formation of PlsB
78 filaments, which have been found to contain an inner phospholipid core (25, 26)

79 Several lines of evidence are consistent with this model. As already stated, PlsB filaments
80 are enzymatically inactive. Second, *E. coli* maintains a phospholipid surplus: *E. coli* protoplasts can
81 be osmotically expanded before lysis occurs (27, 28), and *E. coli* continues to grow for a short time
82 after phospholipid synthesis is inhibited (29). Third, PlsB is also present in excess: the maximum
83 activity of PlsB far exceeds activity needed to provide *E. coli* with phospholipids (8). Finally, when

84 phospholipid synthesis inhibition is relieved, the rate of phospholipid synthesis is transiently faster
85 than the rate observed during steady-state growth, consistent with a brief period of uninhibited
86 phospholipid synthesis in the absence of a phospholipid surplus (30).

87 However, direct evidence for the PlsB filamentation hypothesis is lacking. PlsB filaments
88 have never been observed in wild-type cells. This is likely due to the comparatively low abundance
89 of PlsB in *E. coli* (~1000 PlsB/cell (31)). As protein filaments typically assemble in a cooperative
90 manner (*i.e.* the energetic barrier for nucleating a new filament is higher than for extending an
91 existing filament (32)), each cell might have at most 1-2 filaments. From these assumptions and
92 estimates of PlsB filament geometry (26), a filament containing half the total PlsB population would
93 be small (~180 nm) and thus difficult to observe *in situ.* Here, we use fluorescent tagging to
94 determine PlsB localization in wild-type cells. Our observations are consistent with our PlsB
95 filamentation hypothesis: specifically, accumulation of membrane phospholipids triggers PlsB
96 filamentation and inactivation, enabling negative feedback regulation of phospholipid synthesis and
97 coordinating phospholipid synthesis with growth.

98

99

100 # Results

101 ## PlsB localizes as punctate foci during growth.

102 The ability of proteins to assemble into filaments *in vivo* has been identified in several studies by
103 examining libraries of strains expressing fluorescently tagged proteins (33, 34). To enable PlsB
104 localization, we fused a monomeric GFP variant (msGFP2) to the C-terminus of PlsB (35). As
105 protein fusions may perturb localization and protein activity (36), we first investigated whether our
106 fusion influenced PlsB activity. As PlsB is an essential enzyme, any detrimental effects of protein
107 fusion on PlsB activity are expected to be reflected in the growth rate. Furthermore, localization
108 artefacts may also arise when proteins are expressed above native concentrations. To ensure that
109 PlsB-msGFP2 is expressed at native levels and that any localization observed is not a consequence
110 of overexpression, we integrated the *plsB-msGFP2* gene into the chromosome of wild-type *E. coli*
111 (NCM3722) at the *plsB* locus, replacing unlabelled PlsB while retaining transcriptional control by the
112 *plsB* promoter. *E. coli plsB-msGFP2* grew normally in all tested media (**Fig. 2A**). To determine
113 whether our fusion construct perturbs PlsB function or regulation, we quantified both membrane
114 phospholipids and phospholipid intermediates using liquid chromatography coupled with mass
115 spectroscopy (LCMS). The phospholipid composition of *plsB-msGFP2* cultures (determined by
116 phospholipids/OD) and levels of phospholipid synthesis intermediates was identical to the parent
117 NCM3722 strain in multiple conditions (**Fig. 2B**). Next, we quantified PlsB-msGFP2 using LCMS-
118 based targeted proteomics. The abundance of PlsB peptides in *plsB-msGFP2* closely matched
119 those measured in the parent NCM3722 strain, confirming that PlsB-msGFP2 is expressed from the
120 chromosomal *plsB* locus at native levels (**Fig. 2C**). To confirm that msGFP2 labelling does not
121 disrupt mechanisms that prevent overexpressed PlsB from increasing phospholipid content, we
122 compared phospholipid abundance in our *plsB-msGFP2* strain in which we overexpressed PlsB-
123 msGFP2 from a plasmid with NCM3722 overexpressing unmodified PlsB. While both PlsB and
124 PlsB-msGFP2 overexpression slightly decreased total phospholipid abundance, the phospholipid
125 content of the strain overexpressing PlsB-msGFP2 did not substantially differ from the strain
126 overexpressing PlsB (**Fig. 2D**).

127 To determine how PlsB localizes during steady-state growth, we imaged exponential phase
128 *plsB-msGFP2* cells from a defined rich medium culture (MOPS / 0.2% glucose / 0.1% CAS amino
129 acids). Cells were transferred to an agar pad supplemented with the same medium and imaged
130 using live-cell epifluorescence microscopy. Fluorescent foci were found within 95% of the
131 population, with diffuse fluorescence appearing within the cytoplasm (**Fig. 3A&B**). Most PlsB foci
132 localized at the cell poles (**Fig. 3C**). PlsB foci were present at comparable levels in all growth
133 medium tested, indicating that foci are not an artefact of a specific condition. To determine whether
134 foci localization is an artefact caused by the msGFP2 fluorescent tag, we also imaged PlsB
135 localization using a C-terminal HaloTag fusion. PlsB-HaloTag also localized as punctate foci at a
136 similar frequency as PlsB-msGFP2 (**Fig. 3D**). Finally, we exchanged msGFP2 with the HA epitope
137 and imaged PlsB using immunofluorescence. PlsB-HA was expressed from a plasmid in wild-type
138 NCM3722 cells that were subsequently fixed and imaged with anti-HA antibodies. Overexpressed
139 PlsB-HA also localized as punctate foci in wild-type NCM3722 (**Fig. 3E**). Thus, PlsB foci are not an
140 artefact of specific tags or overexpression.

141 Fluorescence intensity of PlsB foci increases with PlsB expression.

142 The observation that fluorescently tagged proteins localize as foci is consistent with
143 assembly into filaments or other structures such as chemotaxis receptor arrays (37). In many cases,
144 the degree of oligomerization is dependent upon protein concentration, with increased
145 oligomerization correlating with increased protein concentrations. In contrast, if the number or size
146 of foci do not correlate with protein expression, any foci detected may not indicate protein
147 oligomers. For instance, the primary phospholipid synthesis enzyme in *Bacillus subtilis,* PlsX,
148 localizes as foci in some conditions, but foci number did not increase in parallel with PlsX
149 expression (38). To determine whether the PlsB foci represent protein oligomers, we expressed the
150 PlsB-msGFP fusion from a plasmid-borne inducible promoter in our *plsB-msGFP2* strain. Inducing
151 expression of PlsB-msGFP2 did not increase the number of fluorescent foci observed but
152 dramatically increased the foci brightness (**Fig. 3F**), consistent with PlsB foci indicating formation of

153 an oligomeric complex. Thus, the effects of increased PlsB-msGFP2 expression are also consistent
154 with assembly of multimeric complexes.

155 C-terminal tagging may perturb formation of long filament structures.

156 The foci observed following overexpression of PlsB-msGFP2 did not appear as elongated filaments
157 as expected from previous studies (**Fig. 3F**). To determine whether the GFP fusion affects the
158 formation of filaments, we overexpressed unlabeled PlsB in the *plsB-msGFP2* strain and imaged
159 our cells using confocal microscopy. In contrast to the foci detected within cells overexpressing
160 PlsB-msGFP2 alone, we observed linear fluorescent structures more consistent with filaments (**Fig.
161 3G**). This implies that the presence of a C-terminal tag may adversely affect either the assembly of
162 PlsB into an orderly filamentous array or the parallel packing of multiple PlsB filaments. However,
163 immunofluorescence imaging of overexpressed PlsB-HA also appear as foci. Thus, modification of
164 PlsB on the C-terminus may affect the assembly of PlsB filaments.

165 Inhibition of fatty acid synthesis delocalizes PlsB.

166 Despite the unclear effect of C-terminal tagging on the formation of orderly PlsB filaments, the
167 consistent foci-forming behaviour of PlsB is consistent with assembly into some oligomeric
168 structure. However, the functional relevance of the foci is unclear. Fluorescent tagging often
169 introduces artefacts that do not reflect the native location of untagged proteins (39, 40). One
170 approach for testing connections between foci formation and enzyme function is to determine
171 whether foci formation is responsive to metabolic perturbations linked with the function of the
172 enzyme (41). Specifically, if the PlsB foci we observe reflect oligomerization in response to
173 phospholipid membrane abundance, perturbations to membrane abundance or phospholipid
174 metabolism are expected to affect localization. Conversely, if the PlsB foci instead are the
175 consequence of a labelling artefact (e.g. fusion-induced aggregation), the PlsB foci are expected to
176 be unresponsive to perturbations in membrane metabolism.

177 We tested whether PlsB localization is relevant to its physiological function by inhibiting fatty
178 acid synthesis. Triclosan is a fatty acid synthesis inhibitor that acts on the 2*E*-enoyl-acyl-ACP
179 reductase FabI (42). Triclosan was added to cells growing in liquid culture, which were

180 subsequently transferred to an agar pad also containing growth medium and triclosan for live-cell
181 imaging. Triclosan greatly reduced the number of PlsB foci and delocalized fluorescence throughout
182 the cytoplasm (**Fig. 4A**). A similar result was obtained using the fatty acid synthesis inhibitor
183 cerulenin, which inactivates the β-keto-acyl-ACP synthases FabB and FabF (43). To determine
184 whether PlsB foci respond to milder perturbations of fatty acid synthesis, we overexpressed the *E.*
185 *coli* thioesterase TesA without its periplasmic trafficking signal. When localized to the cytoplasm,
186 TesA hydrolyses long-chain fatty acid thioesters (including acyl-ACP PlsB substrates) (44) and
187 reduces the abundance of membrane phospholipids (45) while allowing growth to continue.
188 Overexpression of TesA in *plsB-msGFP2* dispersed PlsB-msGFP2 and reduced the foci count (**Fig.**
189 **4A**). To determine whether PlsB foci dispersal is caused by generic cell growth arrest rather than a
190 specific consequence of fatty acid synthesis inhibition, we imaged *plsB-msGFP2* after adding
191 protein translation inhibitors chloramphenicol and mupirocin. Cells treated with either translation
192 inhibitor ceased to grow but retained PlsB foci (**Fig. 4B**), indicating that PlsB delocalization is not a
193 generic response to growth arrest but is a consequence of fatty acid synthesis inhibition. Thus, PlsB
194 consistently delocalizes in response to perturbations in fatty acid and phospholipid synthesis.

195 The cytoplasmic localization of PlsB observed when phospholipid synthesis is inhibited is
196 unexpected. While PlsB is a peripheral membrane protein and not integrated into the membrane, it
197 is generally regarded as associating stably with the membrane. To further investigate PlsB
198 localization with higher spatial resolution, we imaged triclosan-treated *plsB-msGFP2* using confocal
199 microscopy. Consistent with observations from our wide-field images, PlsB-msGFP2 in triclosan-
200 treated cells is also cytoplasmic and not membrane-associated (**Fig. 4C**). We note that the
201 phosphatidylserine synthesis enzyme PssA is also a peripheral membrane enzyme that reversibly
202 associates with the membrane in response to electrostatic charge and substrate availability (46).

203 PlsB foci gradually reform after phospholipid synthesis is restored.

204 We next tested whether resumption of fatty acid synthesis might cause PlsB foci to reform.
205 Triclosan-treated cells in liquid culture were pelleted, resuspended in fresh medium, and plated on
206 agar containing growth medium and imaged over time. Growth resumed immediately upon triclosan

207 removal, while PlsB remained dispersed at the beginning of imaging. However, after ~30 minutes of
208 growth, foci reappeared, coincident with the time of first cell division (**Fig. 4D**). Foci reappearance is
209 highly synchronized across the population. Thus, both formation and dispersion of PlsB are
210 reversible and responsive to phospholipid metabolism.

211 To further investigate PlsB foci formation, we restarted phospholipid synthesis in triclosan-
212 inhibited cells by feeding exogenous fatty acids palmitate and *cis*-vaccenate. Exogenous fatty acids
213 are converted by the fatty acid-CoA ligase FadD to acyl-CoA, which are substrates for phospholipid
214 synthesis by PlsB and PlsC. Fatty acid-fed cells resumed growth at a much slower rate;
215 nevertheless, PlsB foci steadily accumulated in the population, although less synchronized than
216 when phospholipid synthesis is restarted by triclosan removal (**Fig. 4E**). We speculate that the
217 slower growth rate and delayed appearance of foci is due to the inability to synthesize
218 lipopolysaccharides, which require lipid precursors that cannot be supplied or obtained from
219 exogenous fatty acids. Thus, PlsB consistently localizes as foci when membrane synthesis is
220 unperturbed during steady-state growth but disperses when phospholipid abundance is reduced.

221

222

223 # Discussion

224 Indirect evidence from previous studies is consistent with our hypothesis that PlsB activity (and thus
225 phospholipid synthesis) is regulated by reversible filamentation. First, PlsB concentrations in wild-
226 type cells are far above levels required to provide sufficient phospholipids for steady-state growth
227 (1, 8, 47); second, overexpressed PlsB forms enzymatically inactive filaments (25, 26); finally, many
228 metabolic proteins assemble into enzymatically inactive filaments in the presence of their products
229 (32, 48). Our observations from live-cell imaging experiments support our hypothesis: PlsB localizes
230 as a combination of foci and distributed fluorescence, consistent with the formation of a non-
231 diffusive, membrane-associated state such as a filament. Furthermore, PlsB foci intensity varies in
232 proportion with PlsB expression, consistent with increased PlsB oligomerization, and contrasts with
233 results obtained from fluorescently labelled PlsX in *B. subtilis* cells (38). However, while fluorescent
234 foci are consistent with our hypothesis, many other mechanisms (natural and artefactual) also cause
235 labelled proteins to appear as foci (36). Thus, our strongest evidence is that PlsB localization
236 responds reversibly to membrane abundance in a manner predicted by our hypothesis. Specifically,
237 PlsB foci disappear when membrane phospholipids are depleted and reappear when phospholipid
238 limitation is alleviated.

239 While our live-cell microscopy data support our hypothesis, some questions remain. First,
240 the foci that we observe may not necessarily indicate the formation of PlsB filaments. For instance,
241 the foci may simply reflect increased localization of PlsB monomers or dimers rather than an
242 oligomeric structure. This may be due to a preference for binding in regions of anionic phospholipids
243 or for the curved membrane at the cell poles. Issues also arise from our use of protein fusions to
244 localize PlsB in live cells. C-terminal fusions appear to compromise filament formation. This may be
245 caused by the C-terminal extensions disrupting contacts or tweaking the alignment of monomers
246 and preventing helical packing observed in untagged PlsB. Alternatively, C-terminal tagging may
247 disrupt the arrangement of multiple PlsB filaments into parallel bundles. Unfortunately, solutions
248 such as appending tags to the N-terminus, or inserting a tag in an unstructured loop (an approach
249 successfully used to study MreB localization (49)) are not straightforward to apply to PlsB: the N-

250 terminus lies at the interface with the membrane, and the Alphafold-predicted structure of PlsB does
251 not reveal any obvious unstructured loops that might allow the insertion of a bulky fluorescent label
252 (although a smaller label may be tolerated). Interestingly, although formation of orderly filaments
253 appears to be disrupted, C-terminal tagging does not dramatically affect PlsB function or regulation:
254 growth rate and phospholipid abundance of *plsB-msGFP2* are unaffected. This may even be
255 interpreted as an indication that PlsB and phospholipid homeostasis do *not* in fact rely upon PlsB
256 filamentation. However, multiple studies that have established the role of filamentation in regulation
257 of other metabolic enzymes found that disabling filamentation caused surprisingly subtle effects
258 upon fitness: for instance, disrupting glucokinase filamentation lowered fitness only during growth
259 transitions, not during steady-state growth (41).

260 To directly test whether filamentation is required for membrane synthesis regulation, PlsB
261 mutants that are unable to form filaments should be created and tested *in vivo*. Unfortunately, a
262 single helical turn of a PlsB filament requires more PlsB monomers (25, 26) than current oligomer
263 structure prediction tools allow (50). Thus, PlsB filament structures must be experimentally
264 determined at sufficient resolution to identify residues that stabilize filaments. Expression of
265 filamentation-deficient PlsB mutants would be expected to increase the phospholipid/protein ratio
266 well above wild-type levels would provide additional direct support for our hypothesis. Furthermore,
267 experiments with lipid bilayers supported by a flexible surface could determine whether PlsB
268 filaments are nucleated by extruded lipid filaments, an approach used to study membrane
269 remodelling by BAR proteins (51).

270

271

272 # Methods

273 ## Strains and growth conditions.

274 *Escherichia coli* K-12 strain NCM3722 (CGSC #12355) was used for all experiments. Plasmids and
275 primers used are listed in Tables 1 and 2, respectively, while the amino acid sequences of protein
276 fusions created are in Table 3. *plsB-msGFP2* was cloned into BglBrick plasmid pBbE5k, sub-cloned
277 into pDHL940 to fuse with a kanamycin resistance gene, and subsequently inserted together with
278 the resistance cassette into the NCM3722 chromosome by lambda-red recombination (52). The
279 kanamycin resistance cassette was subsequently removed. The *plsB-HaloTag* strain was
280 constructed in a similar manner. Cells were cultured on MOPS minimal media (53) with 0.2% w/v
281 carbon source (glucose, glycerol, or acetate) or with 0.2% glucose and 0.1% CAS amino acids.
282 Growth was monitored with optical density measurements (Ultrospec 10 Cell Density Meter, GE
283 Healthcare). For microscopy experiments, 5 mL cultures were incubated at 37°C in while rotating at
284 400 rpm. For cultures prepared for experiments requiring larger volumes (growth rate
285 measurements and LCMS analysis), cells were grown in Erlenmeyer flasks containing a magnetic
286 stir bar. Culture flasks were partially submerged in in a Grant Instruments Sub Aqua Pro water bath
287 maintained at 37 °C and stirred (1200 rpm) with submerged 2mag MIXdrive 1 Eco and MIXcontrol
288 20 stir plates. PlsB expression plasmids (PlsB, PlsB-msGFP2, and PlsB-HA) were constructed by
289 inserting the PlsB or PlsB fusion gene into a pBbE5k backbone (54).

290 ## Culture sampling and LCMS analysis.

291 1 mL samples were rapidly removed from exponential-phase cultures and quenched by pipetting
292 immediately into ice-cooled tubes containing 0.25 mL 10% trichloroacetic acid. Quenched cells were
293 pelleted and stored at -80 °C until analysis. LCMS methods used for phospholipid and PlsB
294 quantification are fully described in reference (8).

295 ## Live-cell fluorescence microscopy.

296 The cultures used for microscopy were prepared at outline in the “culture conditions” section. To
297 ensure the bacteria grow during the imaging they were placed on agar pads. To make these pads,
298 first a larger batch of agarose was prepared using 1.5 g low gelling point agarose dissolved in 50

299 mL milli-Q water for a final concentration of 3%. This agar was then autoclaved to ensure sterility.
300 Afterwards, the full volume was divided into 0.5 mL aliquots which were stored at -20°C. For each
301 experiment, one of these aliquots was used and remelted at 80 °C in a heating block. Once melted,
302 0.5 mL of a MOPS medium prepared at 2x concentration is added. The solution is mixed through
303 vortexing and briefly (less than 5 min) placed back in the heating block to ensure it does not gel in
304 the tube. Three 15 x 15 mm glass coverslips are place on a flat piece of parafilm and 0.3 mL of agar
305 is pipetted on each of these. A second coverslip is then gently placed on top of the agar droplet,
306 spreading it out to a (near) uniform shape. These are covered and left to gel, after they have
307 solidified they are placed at 37 °C to pre-heat.

308 Microscopy slides were prepared in two different ways, depending on the microscope used.
309 For widefield fluorescence microscopy, a prepared and pre-heated agar pad is taken and one of the
310 coverslips peeled off. A small amount of culture (1 – 2 µL) is then placed onto the agar pad, which is
311 then placed agar side down onto a larger 22 x 50 mm coverslip. If used for a timelapse, the sides
312 are sealed to prevent drying of the agar pad during the acquisition. For confocal microscopy there is
313 a slight variation on the above protocol, instead of placing the agar onto a 22 x 50 mm coverslip,
314 they are instead placed onto a microscopy dish with a lid and a small amount of wet tissue paper
315 inside to prevent dessication.

316 Widefield microscopy was done initially on an Inverted Olympus IX81 equipped with
317 a Andor Luca R camera (EM-CCD, 104x1002 pixel chip size, 8x8µm pixel size, 14-bit dynamic
318 range, 65% quantum efficiency at 600nm), CoolLED pE-4000 fluorescence excitation source, 100x
319 1.45 NA oil objective (0.13 mm WB), GFP filter cube (ET-EGFP, 470/40 excitation filter, T515lp
320 dichroic filter cut-off, 525/50 emission filter, reference: C229863), phase ring and heating box. The
321 microscope was heated to 37°C before the start of the experiment, at least 30 minutes in advance
322 to ensure a stable temperature. At the start of acquisition the 10x or 20x objective was used to
323 check alignment of the phase ring and make adjustments if needed. Positions were chosen keeping
324 in mind a sufficient number of cells in the field of view and no or minimal non-cell debris. Images
325 were taken in two channels, one in phase contrast (50 ms exposure) and one for GFP

326 (1000 ms exposure, 490 nm, 40% intensity). Phase contrast imaged were taken through the GFP
327 filter cube to save time switching blocks. Where relevant, Z-stacks were taken using a 0.2 µm
328 interval between slices. For timelapses, multiple positions are marked and imaged at 2.5
329 minute intervals, generally for at least 4 hours but up to 8 hours.

330 Confocal microscopy is done on a Nikon Eclipse Ti microscope with a 488 nm laser
331 (confocal-CW, 16 mW), a 100x SR Apo TIRF 1.49 NA oil objective (0.12 mm WB), a 482/35
332 fluorescence emission filter, a EM-CCD Andor iXon X3 DU897 detection device (512x512 pixel chip
333 size, 16x16 µm pixel size, 14 bit dynamic range, >90% quantum efficiency at 600nm), and Tokai Hit
334 sample incubator chamber. The sample is incubated at 37°C during imaging. Suitable locations are
335 found by looking at the sample using the Resonant scanning. Once a position is found a high
336 resolution image is taken using Galvano scanning.

337 HaloTag imaging.

338 Cultures of *plsB-HaloTag* grown to OD600 of ~0.6, incubated with 250 nM JF635 dye for 1 hour at
339 37 °C, and washed three times with medium before imaging.

340 Immunofluorescence.

341 An NCM3722 pBbE5K-PlsB-HA culture was induced with 100 µM IPTG and grown for
342 approximately 1 hour until OD600 of 0.3 – 0.4. Following a gentle fixation protocol (55), the cells
343 were subsequently fixed for 15 minutes with formaldehyde and glutaraldehyde (final concentrations
344 2.8% and 0.04%, respectively), washed twice with PBS and concentrated 100-fold by centrifugation
345 and resuspension in PBS. The dense cell suspension was incubated for 45 min with 1% Triton X-
346 100 and washed three times with 150 µL PBS. Next, the cells are incubated 45 min in 150 µL PBS
347 containing 100 µg/mL lysozyme and 5 mM EDTA, followed by three washes with 150 µL PBS and
348 stored at -20°C until ready for labelling. For antibody labelling, cells were incubated for 1 hour at 37
349 °C with 0.5 mg/mL antibody (anti-HA rabbit recombinant monoclonal antibody labeled with Alexa
350 Fluor 488, Abcam EPR22919-101). Cells are washed three times with 150 µL PBS containing
351 0.05% Tween-20, resuspended in 150 µL PBS and analyzed using fluorescence microscopy.

352 **Image analysis.**

353 To augment the qualitative analysis of microscopy images we developed an image analysis
354 pipeline. The primary goal of this pipeline is to count the number of foci within each cell. This
355 requires detection of individual cells and the subsequent detection of the foci within each cell. The
356 first step is to create image stacks of both the phase contrast and fluorescent images separately.
357 The phase contrast images are loaded into Fiji. The MicrobeJ plugin (56) is then used to segment
358 the cells. The first segmentation is automatic, and this is then followed by manual refinement where
359 necessary. Manual refinement is almost exclusively reserved for eliminating false positives or for
360 separating touching cells. Cells touching the edge are discarded and for all remaining cells the
361 coordinates of their contours are exported. Next, both these contours and the fluorescent images
362 stack are loaded into a custom-made Matlab script. Here the contours are used to find each
363 individual cell in the fluorescent images. All other pixels not defined as cell are considered
364 background and the average background value is subtracted across the image. Next, each cell is
365 analyzed individually. First the cytoplasmic background is estimated by taking the median intensity
366 of cell. This value is then multiplied with a set factor (1.7) to create a threshold. All pixels higher than
367 this threshold are located and further filtered on cluster size. Only clusters of more than 5 pixels are
368 considered a foci. From this we can then collect the number of foci per cell, the number of pixels
369 (i.e. size) and the total intensity of the foci. Next, the centroid of the cell is found as well as the
370 centroid of each foci to determine where in the cell they are located. Besides the exact location of
371 each foci, they are also classified as polar or non-polar. For this determination, foci are considered
372 to be located at the poles when located at the outer 10% of the cell length on either end. Finally, the
373 cell length and width are also measured. All this data is then collected and exported for further
374 analysis.

375 # Acknowledgements

376 We thank Mehmet Berkmen for sharing HaloTag plasmid pDHL940, Carlas Smith and Michal
377 Shemesh for expertise and assistance with microscopy, Jeremie Capoulade for performing pilot
378 experiments, and Tanneke den Blaauwen and Jolanda Verheul for assistance with cell fixation and

379 immunofluorescence. We thank Ariane Briegel and Arjen Jakobi for encouragement and insightful
380 suggestions, and the entire Bokinsky Lab for stimulating discussions and support.

381 Author Contributions

382 JB: designed and performed experiments, built image analysis pipeline, evaluated data. DF:
383 collected samples for LCMS experiments. MG: constructed *plsB-HaloTag* strain and performed
384 HaloTag imaging experiments. AS: performed initial experiments confirming TesA-driven PlsB
385 delocalization. AZ-D: LCMS analysis. GB: supervised project, constructed *plsB-msGFP2* strain,
386 evaluated data. JB and GB wrote the manuscript. All authors approved the final manuscript.

387

388

References

1. Dowhan W. 2013. A retrospective: use of Escherichia coli as a vehicle to study phospholipid synthesis and function. Biochim Biophys Acta 1831:471–494.

2. Yao J, Rock CO. 2013. Phosphatidic acid synthesis in bacteria. Biochim Biophys Acta Mol Cell Biol Lipids https://doi.org/10.1016/j.bbalip.2012.08.018.

3. Yoshimura M, Oshima T, Ogasawara N. 2007. Involvement of the YneS/YgiH and PlsX proteins in phospholipid biosynthesis in both Bacillus subtilis and Escherichia coli. BMC Microbiol 7:69.

4. Ruiz N, Davis RM, Kumar S. 2021. YhdP, TamB, and YdbH Are Redundant but Essential for Growth and Lipid Homeostasis of the Gram-Negative Outer Membrane. mBio 12.

5. Goelz SE, Cronan Jr. JE. 1980. The positional distribution of fatty acids in Escherichia coli phospholipids is not regulated by sn-glycerol 3-phosphate levels. J Bacteriol 144:462–464.

6. Davis MS, Solbiati J, Cronan JE. 2000. Overproduction of acetyl-CoA carboxylase activity increases the rate of fatty acid biosynthesis in Escherichia coli. Journal of Biological Chemistry 275:28593–28598.

7. Heath RJ, Jackowski S, Rock CO. 1994. Guanosine Tetraphosphate Inhibition of Fatty-Acid and Phospholipid-Synthesis in Escherichia coli Is Relieved by Overexpression of Glycerol-3-Phosphate Acyltransferase (PlsB). Journal of Biological Chemistry 269:26584–26590.

8. Noga MJ, Büke F, van den Broek NJF, Imholz NCE, Scherer N, Yang F, Bokinsky G. 2020. Posttranslational Control of PlsB Is Sufficient To Coordinate Membrane Synthesis with Growth in Escherichia coli. mBio 11:e02703-19.

9. Snider MD. 1979. Control of membrane lipid synthesis in Escherichia coli during growth and during the stringent response. J Biol Chem 254:7202–7917.

10. Wilkison WO, Walsh JP, Corless JM, Bell RM. 1986. Crystalline arrays of the Escherichia coli sn-glycerol-3-phosphate acyltransferase, an integral membrane protein. Journal of Biological Chemistry 261:9951–9958.

11. Rock CO, Goelz SE, Cronan JE. 1981. Phospholipid synthesis in Escherichia coli. Characteristics of fatty acid transfer from acyl-acyl carrier protein to sn-glycerol 3-phosphate. Journal of Biological Chemistry 256.

12. Green PR, Merrill Jr. AH, Bell RM. 1981. Membrane phospholipid synthesis in Escherichia coli. Purification, reconstitution, and characterization of sn-glycerol-3-phosphate acyltransferase. Journal of Biological Chemistry 256:11151–11159.

13. Green PR, Bell RM. 1984. Asymmetric reconstitution of homogenous Escherichia coli sn-glycerol-3-phosphate acyltransferase into phospholipid vesicles. Journal of Biological Chemistry 259:14688–14694.

14. Scheideler MA, Bell RM. 1989. Phospholipid dependence of homogeneous, reconstituted sn-glycerol-3-phosphate acetyltransferase of Escherichia coli. Journal of Biological Chemistry.

15. Scheideler MA, Bell RM. 1991. Characterization of active and latent forms of the membrane-associated sn-glycerol-3-phosphate acyltransferase of Escherichia coli. Journal of Biological Chemistry.

16. Wilkison WO, Bell RM, Taylor KA, Costello MJ. 1992. Structural characterization of ordered arrays of sn-glycerol-3-phosphate acyltransferase from Escherichia coli. J Bacteriol 174:6608–6616.

17. Simonet JC, Burrell AL, Kollman JM, Peterson JR. 2020. Freedom of assembly: Metabolic enzymes come together. Mol Biol Cell https://doi.org/10.1091/MBC.E18-10-0675.

18. Park CK, Horton NC. 2019. Structures, functions, and mechanisms of filament forming enzymes: a renaissance of enzyme filamentation. Biophys Rev https://doi.org/10.1007/s12551-019-00602-6.

19. Narayanaswamy R, Levy M, Tsechansky M, Stovall GM, O'Connell JD, Mirrielees J, Ellington AD, Marcotte EM. 2009. Widespread reorganization of metabolic enzymes into reversible assemblies upon nutrient starvation. Proc Natl Acad Sci U S A 106.

20. Noree C, Begovich K, Samilo D, Broyer R, Monfort E, Wilhelm JE. 2019. A quantitative screen for metabolic enzyme structures reveals patterns of assembly across the yeast metabolic network. Mol Biol Cell 30.

21. Barry RM, Bitbol AF, Lorestani A, Charles EJ, Habrian CH, Hansen JM, Li HJ, Baldwin EP, Wingreen NS, Kollman JM, Gitai Z. 2014. Large-scale filament formation inhibits the activity of CTP synthetase. Elife 3:1–19.

22. Stoddard PR, Lynch EM, Farrell DP, dosey AM, diMaio F, Williams TA, Kollman JM, Murray AW, Garner EC. 2020. Polymerization in the actin ATPase clan regulates hexokinase activity in yeast. Science (1979) 367:1039–1042.

23. Davidi D, Milo R. 2017. Lessons on enzyme kinetics from quantitative proteomics. Curr Opin Biotechnol https://doi.org/10.1016/j.copbio.2017.02.007.

24. Staykova M, Holmes DP, Read C, Stone HA. 2011. Mechanics of surface area regulation in cells examined with confined lipid membranes. Proc Natl Acad Sci U S A 108:9084–9088.

25. Wilkison WO, Walsh JP, Corless JM, Bell RM. 1986. Crystalline arrays of the Escherichia coli sn-glycerol-3-phosphate acyltransferase, an integral membrane protein. Journal of Biological Chemistry 261:9951–9958.

26. Wilkison WO, Bell RM, Taylor KA, Costello MJ. 1992. Structural characterization of ordered arrays of sn-glycerol-3-phosphate acyltransferase from Escherichia coli. J Bacteriol 174:6608–6616.

27. Sun Y, Sun TL, Huang HW. 2014. Physical properties of Escherichia coli spheroplast membranes. Biophys J 107:2082–2090.

28. Buda R, Liu Y, Yang J, Hegde S, Stevenson K, Bai F, Pilizota T. 2016. Dynamics of Escherichia coli's passive response to a sudden decrease in external osmolarity. Proc Natl Acad Sci U S A 113:E5838–E5846.

29. Bell RM. 1974. Mutants of Escherichia coli defective in membrane phospholipid synthesis: macromolecular synthesis in an sn glycerol 3 phosphate acyltransferase K(m) mutant. J Bacteriol 117.

30. McIntyre TM, Chamberlain BK, Webster RE, Bell RM. 1977. Mutants of Escherichia coli defective in membrane phospholipid synthesis. Effects of cessation and reinitiation of phospholipid synthesis on macromolecular synthesis and phospholipid turnover. Journal of Biological Chemistry 252:4487–4493.

31. Li GW, Burkhardt D, Gross C, Weissman JS. 2014. Quantifying absolute protein synthesis rates reveals principles underlying allocation of cellular resources. Cell 157:624–635.

32. Barry RM, Bitbol AF, Lorestani A, Charles EJ, Habrian CH, Hansen JM, Li HJ, Baldwin EP, Wingreen NS, Kollman JM, Gitai Z. 2014. Large-scale filament formation inhibits the activity of CTP synthetase. Elife 3:1–19.

33. Narayanaswamy R, Levy M, Tsechansky M, Stovall GM, O'Connell JD, Mirrielees J, Ellington AD, Marcotte EM. 2009. Widespread reorganization of metabolic enzymes into reversible assemblies upon nutrient starvation. Proc Natl Acad Sci U S A 106.

34. Noree C, Begovich K, Samilo D, Broyer R, Monfort E, Wilhelm JE. 2019. A quantitative screen for metabolic enzyme structures reveals patterns of assembly across the yeast metabolic network. Mol Biol Cell 30.

35. Valbuena FM, Fitzgerald I, Strack RL, Andruska N, Smith L, Glick BS. 2020. A photostable monomeric superfolder green fluorescent protein. Traffic 21:534–544.

36. Margolin W. 2012. The price of tags in protein localization studies. J Bacteriol https://doi.org/10.1128/JB.01640-12.

37. Thiem S, Sourjik V. 2008. Stochastic assembly of chemoreceptor clusters in Escherichia coli. Mol Microbiol 68.

38. Sastre DE, Bisson-Filho A, de Mendoza D, Gueiros-Filho FJ. 2016. Revisiting the cell biology of the acyl-ACP: Phosphate transacylase PlsX suggests that the phospholipid synthesis and cell division machineries are not coupled in Bacillus subtilis. Mol Microbiol 100:621–634.

39. Ghodke H, Caldas VEA, Punter CM, van Oijen AM, Robinson A. 2016. Single-Molecule Specific Mislocalization of Red Fluorescent Proteins in Live Escherichia coli. Biophys J 111.

40. Swulius MT, Jensen GJ. 2012. The helical mreb cytoskeleton in Escherichia coli MC1000/pLE7 is an artifact of the N-terminal yellow fluorescent protein tag. J Bacteriol 194:6382–6386.

41. Stoddard PR, Lynch EM, Farrell DP, dosey AM, diMaio F, Williams TA, Kollman JM, Murray AW, Garner EC. 2020. Polymerization in the actin ATPase clan regulates hexokinase activity in yeast. Science (1979) 367:1039–1042.

42. Heath RJ, Rubin JR, Holland DR, Zhang E, Snow ME, Rock CO. 1999. Mechanism of triclosan inhibition of bacterial fatty acid synthesis. Journal of Biological Chemistry 274:11110–11114.

43. D'Agnolo G, Rosenfeld IS, Awaya J, Omura S, Vagelos PR. 1973. Inhibition of fatty acid synthesis by the antibiotic cerulenin. Specific inactivation of beta-ketoacyl-acyl carrier protein synthetase. Biochim Biophys Acta 326:155–156.

44. Bonner WM, Bloch K. 1972. Purification and properties of fatty acyl thioesterase I from Escherichia coli. Journal of Biological Chemistry 247.

45. Cho H, Cronan JE. 1995. Defective export of a periplasmic enzyme disrupts regulation of fatty acid synthesis. Journal of Biological Chemistry https://doi.org/10.1074/jbc.270.9.4216.

46. Louie K, Chen YC, Dowhan W. 1986. Substrate-induced membrane association of phosphatidylserine synthase from Escherichia coli. J Bacteriol https://doi.org/10.1128/jb.165.3.805-812.1986.

47. Wilkison WO, Bell RM. 1997. sn-Glycerol-3-phosphate acyltransferase from Escherichia coli. Biochimica et Biophysica Acta (BBA) - Lipids and Lipid Metabolism 1348:3–9.

48. Park CK, Horton NC. 2019. Structures, functions, and mechanisms of filament forming enzymes: a renaissance of enzyme filamentation. Biophys Rev https://doi.org/10.1007/s12551-019-00602-6.

49. Bendezú FO, Hale CA, Bernhardt TG, De Boer PAJ. 2009. RodZ (YfgA) is required for proper assembly of the MreB actin cytoskeleton and cell shape in E. coli. EMBO Journal 28.

50. Abramson J, Adler J, Dunger J, Evans R, Green T, Pritzel A, Ronneberger O, Willmore L, Ballard AJ, Bambrick J, Bodenstein SW, Evans DA, Hung C-C, O'Neill M, Reiman D, Tunyasuvunakool K, Wu Z, Žemgulytė A, Arvaniti E, Beattie C, Bertolli O, Bridgland A, Cherepanov A, Congreve M, Cowen-Rivers AI, Cowie A, Figurnov M, Fuchs FB, Gladman H, Jain R, Khan YA, Low CMR, Perlin K, Potapenko A, Savy P, Singh S, Stecula A, Thillaisundaram A, Tong C, Yakneen S, Zhong ED, Zielinski M, Žídek A, Bapst V, Kohli P, Jaderberg M, Hassabis D, Jumper JM. 2024. Accurate structure prediction of biomolecular interactions with AlphaFold 3. Nature 630:493–500.

51. Le Roux AL, Tozzi C, Walani N, Quiroga X, Zalvidea D, Trepat X, Staykova M, Arroyo M, Roca-Cusachs P. 2021. Dynamic mechanochemical feedback between curved membranes and BAR protein self-organization. Nat Commun 12.

52. Datsenko KA, Wanner BL. 2000. One-step inactivation of chromosomal genes in Escherichia coli K-12 using PCR products. Proc Natl Acad Sci U S A 97:6640–6645.

53. Neidhardt FC, Bloch PL, Smith DF. 1974. Culture Medium for Enterobacteria. J Bacteriol 119:736–747.

54. Lee T, Krupa RA, Zhang F, Hajimorad M, Holtz WJ, Prasad N, Lee S, Keasling JD, Khosla C, Keasling J, Lee S, Chou H, Ham T, Lee T, Keasling J, Atsumi S, Liao J, Raab R, Tyo K, Stephanopoulos G, Pieper D, Reineke W, Martin V, Pitera D, Withers S, Newman J, Keasling J, Pitera D, Paddon C, Newman J, Keasling J, Alper H, Fischer C, Nevoigt E, Stephanopoulos G, Ajikumar P, Xiao W, Tyo K, Wang Y, Simeon F, Leonard E, Mucha O,

Phon T, Pfeifer B, Stephanopoulos G, Dejong J, Liu Y, Bollon A, Long R, Jennewein S, Williams D, Croteau R, Yan Y, Kohli A, Koffas M, Li M, Elledge S, Shao Z, Zhao H, Zhao H, Gibson D, Young L, Chuang R, Venter J, Hutchison C, Smith H, Keasling J, Lee S, Kim H, Park J, Park J, Kim T, Martin C, Nielsen D, Solomon K, Prather K, Canton B, Labno A, Endy D, Knight T, Anderson J, Dueber J, Leguia M, Wu G, Goler J, Arkin A, Keasling J, Shetty R, Endy D, Knight T, Tao L, Jackson R, Cheng Q, Anthony J, Anthony L, Nowroozi F, Kwon G, Newman J, Keasling J, Lee S, Newman J, Keasling J, Lee S, Keasling J, Lee S, Keasling J, Guzman L, Belin D, Carson M, Beckwith J, Hajimorad M, Gray P, Keasling J, Lee S, Chou H, Pfleger B, Newman J, Yoshikuni Y, Keasling J, Gorke B, Stulke J, Skulj M, Okrslar V, Jalen S, Jevsevar S, Slanc P, Strukelj B, Menart V, Carapuca E, Azzoni A, Prazeres D, Monteiro G, Mergulhao F, Lee C, Ow D, Oh S, Lee C, Kim J, Shin S, Hwang S, Tao L, Jackson R, Rouviere P, Cheng Q, Lee C, Lee S, Shin S, Hwang S, Friehs K, Antoine R, Locht C, Lutz R, Bujard H, Manen D, Xia G, Caro L, Grabherr R, Bayer K, Glass R, Kues U, Stahl U, Redding-Johanson A, Batth T, Chan R, Krupa R, Szmidt H, Adams P, Keasling J, Lee T, Mukhopadhyay A, Petzold C, Dunlop M, Dossani Z, Szmidt H, Chu H, Lee T, Keasling J, Hadi M, Mukhopadhyay A, Leguia M, Brophy J, Densmore D, Anderson J, Horton R, Cai Z, Ho S, Pease L, Pushnova E, Geier M, Zhu Y, Mason G, Provero P, Vaira A, Accotto G. 2011. BglBrick vectors and datasheets: A synthetic biology platform for gene expression. J Biol Eng 5:12.

55. Buddelmeijer N, Aarsman M, den Blaauwen T. 2013. Immunolabeling of Proteins in situ in Escherichia coli K12 Strains. Bio Protoc 3.

56. Ducret A, Quardokus EM, Brun Y V. 2016. MicrobeJ, a tool for high throughput bacterial cell detection and quantitative analysis. Nat Microbiol 1.

57. Ke N, Landgraf D, Paulsson J, Berkmen M. 2016. Visualization of periplasmic and cytoplasmic proteins with a self-labeling protein tag. J Bacteriol 198.

633 # Figures and Tables

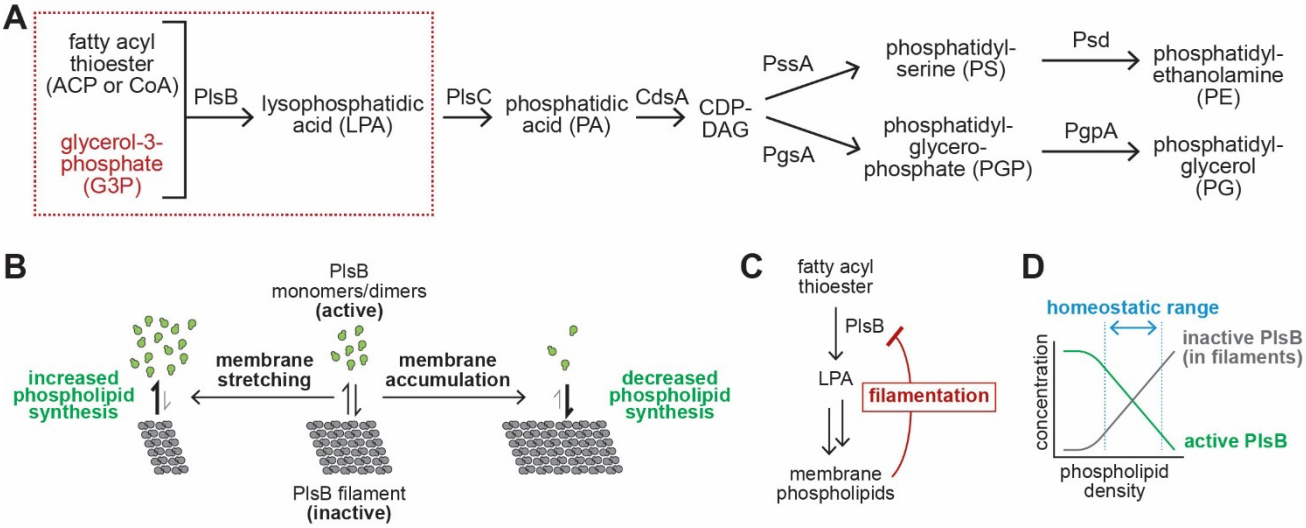

634

635 **Figure 1.** Hypothesized mechanism coordinating membrane phospholipid synthesis with cell growth
636 in *Escherichia coli*. **A.** The role of PlsB in the *E. coli* phospholipid synthesis pathway. **B.** Our
637 hypothesis predicts that during growth, the PlsB population is partitioned between an active form
638 (either monomers or dimers) and inactive protein filaments. We propose that the degree of PlsB
639 filamentation (and thus the level of PlsB activity and the rate of phospholipid synthesis) is
640 determined by the density of phospholipids within the inner membrane: surplus phospholipids
641 increase PlsB filamentation, while decreased phospholipid density (i.e. membrane stretching)
642 decreases PlsB filamentation. This mechanism establishes an effective negative feedback loop that
643 controls PlsB activity **(C)** and that maintains phospholipid density at a homeostatic level **(D)**.

644

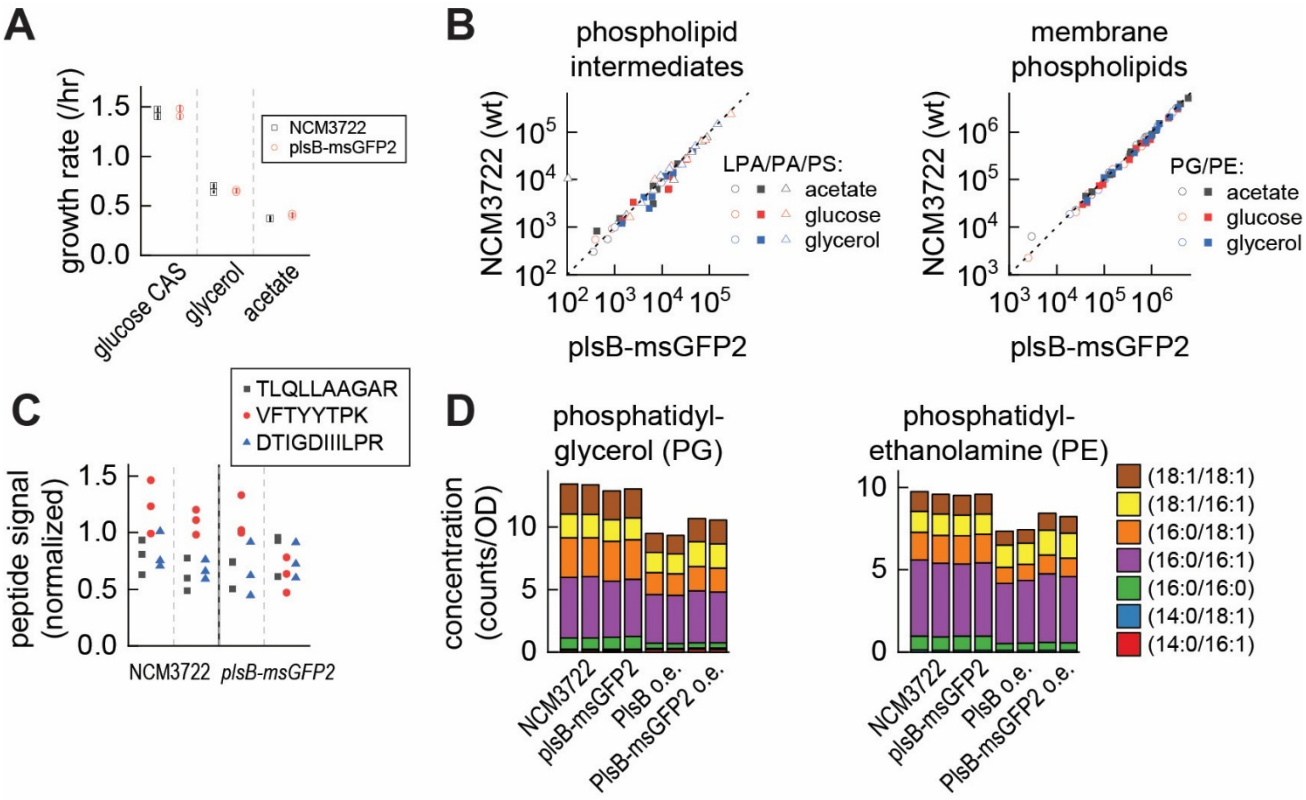

Figure 2. A msGFP2 fusion with PlsB retains activity. **A.** Growth rates of *E. coli* NCM3722 (wild-type) and NCM3722 *plsB-msGFP2* (PlsB-msGFP2 expressed from the chromosomal *plsB* operon) obtained in three defined media. Two biological replicates of each strain in each condition are shown. **B.** Abundance of phospholipid synthesis intermediates (LPA, PA, and PS) and membrane phospholipids (PG and PE) are unaffected by expression of PlsB-msGFP2. Data obtained from one biological replicate in each condition. **C.** Cellular concentration of PlsB-msGFP2 is equivalent to concentration of PlsB in NCM3722. Triplicate data obtained using LCMS-based peptide quantification from two biological replicates of each strain are shown. **D.** Overexpression of PlsB in NCM3722 and PlsB-msGFP2 in *plsB-msGFP2* generate similar membrane phospholipid profiles. Duplicate data from one biological replicate of each condition is depicted.

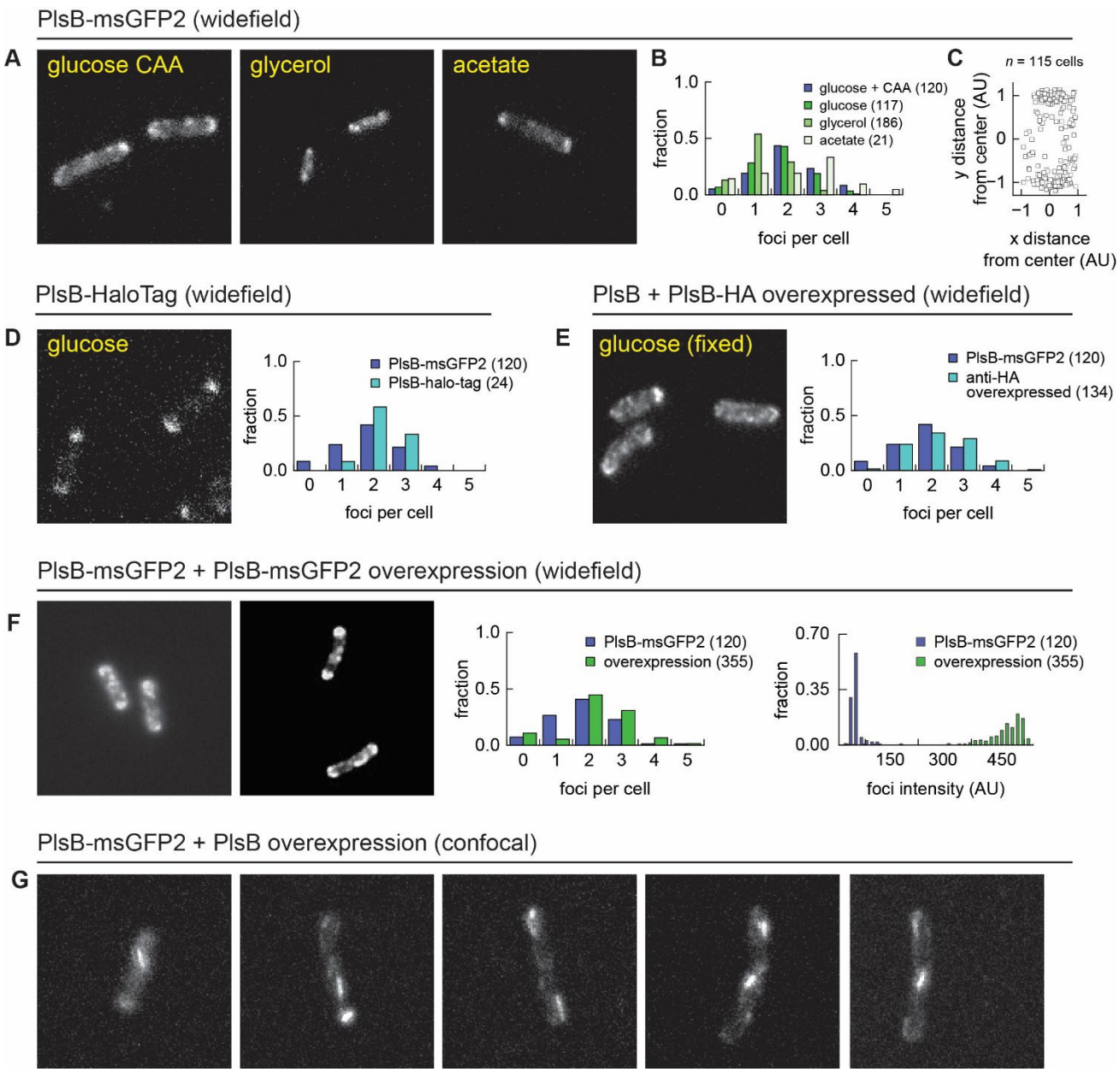

Figure 3. PlsB localizes as foci during steady-state growth. **A.** Live-cell fluorescent microscopy images of *E. coli* NCM3722 *plsB-msGFP2* on agar pads supplemented with defined medium. **B.** PlsB foci form at similar frequencies across conditions and usually localize at cell poles **(C)**. **D.** PlsB foci are also observed with different protein fusions, and in fixed cells **(E)**. **F.** Plasmid-based overexpression of PlsB-msGFP2 does not affect the number of PlsB foci detected per cell but increases the brightness of the foci. **G.** Overexpression of unlabelled PlsB in *plsB-msGFP2* background allows resolution of fluorescent structures resembling filaments. For all panels, the numbers of analysed cells are provided in the figure legends.

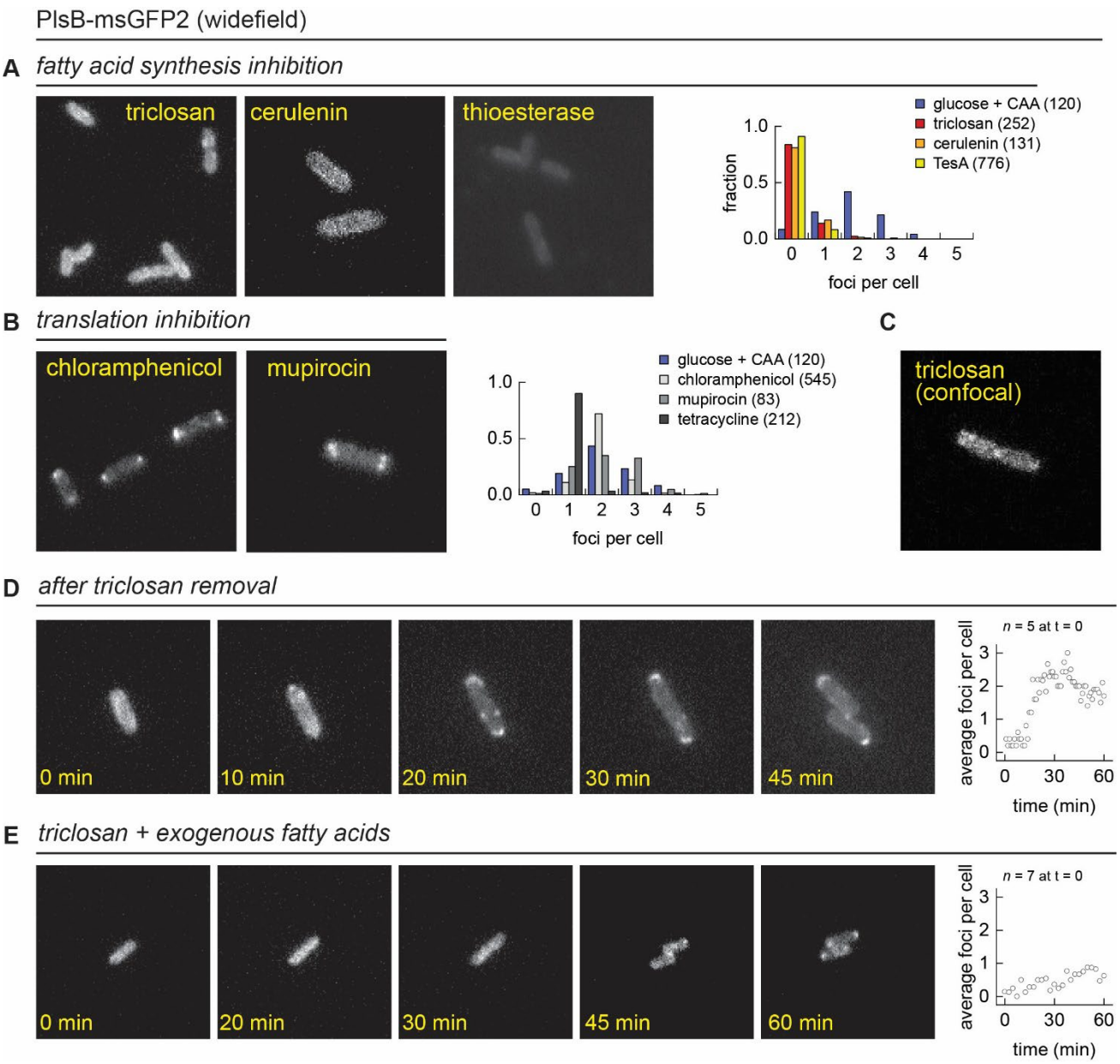

Figure 4. PlsB foci respond dynamically to phospholipid abundance. **A.** PlsB-msGFP2 delocalizes into the cytoplasm after membrane synthesis inhibition. Images of *plsB-msGFP2* cells grown in MOPS/0.2% glucose 0.1% CAS amino acids treated with triclosan, cerulenin, or expressing the thioesterase TesA and transferred to agar pads supplemented with identical medium and antibiotics. **B.** PlsB-msGFP2 foci do not substantially respond to translation inhibitors, indicating that delocalization is not a generic response to growth arrest. **C.** A confocal image of triclosan-treated *plsB-msGFP* suggests that PlsB-msGFP2 delocalizes into the cytoplasm and does not associate with the membrane. **D&E.** PlsB-msGFP2 foci reappear when membrane synthesis is restored by either removing triclosan (**D**) or by adding free fatty acids palmitate and *cis*-vaccenate (**E**). For all panels, the numbers of analysed cells are provided in the figure legends.

Table 1. Plasmids in this study.		
Plasmid	**Role**	**Source**
pQE-60NA-msGFP2	msGFP2 sequence	AddGene (plasmid #135301)
pDHL940	HaloTag sequence and antibiotic cassette for recombination	Mehmet Berkmen (57)
pBbE5k	BglBrick vector (lacUV5 promoter, ColE1 origin, kanamycin resistance marker)	AddGene (plasmid #35279)
pBbA2a	BglBrick vector (pTet promoter, p15a origin, ampicillin resistance marker)	AddGene (plasmid #35325)
pBbE5k-PlsB-msGFP2	PlsB-msGFP2 overexpression	This study
pBbA5a-TesA	Cytoplasmic thioesterase expression	This study
pBbE5k-PlsB	PlsB overexpression	This study
pBbE5k-PlsB-HA	HA-tagged PlsB ovreexpression	This study

680

681

Table 2. Primers used in this study.		
Plasmid or DNA fragment	**primer name**	**sequence**
pBbE5k-PlsB	GB121517-PlsB.f	GCGGATAACAATTTCAGAATTCAAAAGATCT CCAGAGGCTTTACATCGTTTatgTCC
	GB121517-PlsB.r	agatccttactcgagtttggatccttaCCCTTCGCCCTGCGT
	GB121517-plasB.f	ACGCAGGGCGAAGGGtaa ggatccaaactcgagtaaggatct
	GB121517-plasB.r	GGAcatAAACGATGTAAAGCCTCTGGAGATCTTTTGAATT CTGAAATTGTTATCCGC
pBbE5k-PlsB-HaloTag	MG_100818-HaloPlsB_Fpls	ctactctggagatttccggttaaggatccaaactcgagtaaggat
	MG_100818-HaloPlsB_Rpls	ccaccgccaccgctCCCTTCGCCCTGCGT
	MG_100818-HaloPlsB_Fphalo	ACGCAGGGCGAAGGGagcggtggcggtgg
	MG_100818-HaloPlsB_Rphalo	atccttactcgagtttggatccttaaccggaaatctccagagtag
pBbE5k-PlsB-msGFP2	GB20201012-pPlsB-halo.f	GAGGCAGTGGCGGTTCTtaaggatccaaactcgagtaaggatctcc
	GB20201012-pPlsB-halo.r	GTGAACAGGCTCTCAGTGCTATCatcgttactgccaccgc
	GB20201012-msGFPins.f	gcggtggcagtaacgatGATAGCACTGAGAGCCTGTTCAC
	GB20201012-msGFPins.r	ggagatccttactcgagtttggatccttaAGAACCGCCACTGCCTC
pBbE5k-PlsB-HA	GB101022-plsB.BglII.f	AAAAGATCTCCAGAGGCTTTACATCGTTTATG
	GB221014-plsB.HA-L.XhoI.r	TTACTCGAGTTAAGCGTAATCTGGAACATCGTATGGGTA ATCGTTACTGCCACCGCCACC
PlsB-HaloTag chromosomal insertion	MG_091118_Halo Tagplsb_F	CGTGCGTTTGACGATTGAGAGTGCGACGCAGGGCGAA GGGagcggtggcggtggcagtaa
	MG_091118_Halo Tagplsb_R	CGGATAAGGCGTTTTCGCCGCATCCGGCAATTCTCTCT GAattccggggatccgtcgacc
	MG_101918-SOEplsb.F1	ACCTTCTGGTTGTTGAGTGC
	MG_101918-SOEplsb.R1	CTGCGTCGCACTCTCAAT
	MG_101918-SOEplsb.F2	CTGCAAATTCAATAAATTGCGATG
	MG_101918-SOEplsb.R2	GGTGAGTTAAATGGCTTAGGC
PlsB-msGFP2 chromosomal insertion	GB201110-DHL940.f	GAGGCAGTGGCGGTTCTtaatgtaggctggagctgcttc
	GB201110-msGFP2.r	gaagcagctccagcctacattaAGAACCGCCACTGCCTC

	GB201110-msGFP2.f	ttcgctattacgccagctggatgTCCGGCTGGCCACG
	GB201110-DHL940.r	CGTGGCCAGCCGGAcatccagctggcgtaatagcgaa
	MG_101918-SOEplsb.F2	CTGCAAATTCAATAAATTGCGATG
	GB201127-PlsBint.ubiA.rseq	GGCACTGATGGCGATCATC
	GB201127-PlsBint.50del.r	CATCGCAATTTATTGAATTTGCAGattccggggatccgtcgacc
	GB201023.plsBint.f	CGCGAAACGCTGCAACG
pBbA5a-TesA	GB20150313-TesA.f	CAGAATTCAAAAGATCTAGGAGGAAAAAAATG GACACGTTATTGATTCTGGGTGATAG
	GB20150313-TesA.r	gagatccttactcgagtttggatccttaTGAGTCATGATTTACTAAAGG CTGC
	GB20150313-TesA-plas.f	GCAGCCTTTAGTAAATCATGACTCAtaa ggatccaaactcgagtaaggatctc
	GB20150313-TesA-plas.r	CTATCACCCAGAATCAATAACGTGTCCATTTTTTTCCTC CTAGATCTTTTGAATTCTG

682

683

Table 3. Amino acid sequences of PlsB fusions. Linker sequences are underlined while fusion tags are in bold text.

Protein fusion	Amino acid sequence
PlsB-msGFP2	MSGWPRIYYKLLNLPLSILVKSKSIPADPAPELGLDTSRPIMYVLPYNSK ADLLTLRAQCLAHDLPDPLEPLEIDGTLLPRYVFIHGGPRVFTYYTPKE ESIKLFHDYLDLHRSNPNLDVQMVPVSVMFGRAPGREKGEVNPPLR MLNGVQKFFAVLWLGRDSFVRFSPSVSLRRMADEHGTDKTIAQKLAR VARMHFARQRLAAVGPRLPARQDLFNKLLASRAIAKAVEDEARSKKIS HEKAQQNAIALMEEIAANFSYEMIRLTDRILGFTWNRLYQGINVHNAER VRQLAHDGHELVYVPCHRSHMDYLLLSYVLYHQGLVPPHIAAGINLNF WPAGPIFRRLGAFFIRRTFKGNKLYSTVFREYLGELFSRGYSVEYFVE GGRSRTGRLLDPKTGTLSMTIQAMLRGGTRPITLIPIYIGYEHVMEVGT YAKELRGATKEKESLPQMLRGLSKLRNLGQGYVNFGEPMPLMTYLNQ HVPDWRESIDPIEAVRPAWLTPTVNNIAADLMVRINNAGAANAMNLCC TALLASRQRSLTREQLTEQLNCYLDLMRNVPYSTDSTVPSASASELID HALQMNKFEVEKDTIGDIIILPREQAVLMTYYRNNIAHMLVLPSLMAAIV TQHRHISRDVLMEHVNVLYPMLKAELFLRWDRDELPDVIDALANEMQ RQGLITLQDDELHINPAHSRTLQLLAAGARETLQRYAITFWLLSANPSI NRGTLEKESRTVAQRLSVLHGINAPEFFDKAVFSSLVLTLRDEGYISDS GDAEPAETMKVYQLLAELITSDVRLTIESATQGEGSGGGGSND**DSTES LFTGVVPILVELDGDVNGHKFSVRGEGEGDATNGKLTLKFICTTGKLP VPWPTLVTTLTYGVQCFSRYPDHMKQHDFFKSAMPEGYVQERTITFK DDGTYKTRAEVKFEGDTLVNRIELKGIDFKEDGNILGHKLEYNYNSH NVYITADKQKNGIKANFKIRHNVEDGSVQLADHYQQNTPIGDGPVLL PDNHYLSTQSKLSKDPNEKRDHMVLLEFVTAAGITGGSGGS**
PlsB-HA	MSGWPRIYYKLLNLPLSILVKSKSIPADPAPELGLDTSRPIMYVLPYNSK ADLLTLRAQCLAHDLPDPLEPLEIDGTLLPRYVFIHGGPRVFTYYTPKE ESIKLFHDYLDLHRSNPNLDVQMVPVSVMFGRAPGREKGEVNPPLR MLNGVQKFFAVLWLGRDSFVRFSPSVSLRRMADEHGTDKTIAQKLAR VARMHFARQRLAAVGPRLPARQDLFNKLLASRAIAKAVEDEARSKKIS HEKAQQNAIALMEEIAANFSYEMIRLTDRILGFTWNRLYQGINVHNAER VRQLAHDGHELVYVPCHRSHMDYLLLSYVLYHQGLVPPHIAAGINLNF WPAGPIFRRLGAFFIRRTFKGNKLYSTVFREYLGELFSRGYSVEYFVE GGRSRTGRLLDPKTGTLSMTIQAMLRGGTRPITLIPIYIGYEHVMEVGT YAKELRGATKEKESLPQMLRGLSKLRNLGQGYVNFGEPMPLMTYLNQ HVPDWRESIDPIEAVRPAWLTPTVNNIAADLMVRINNAGAANAMNLCC TALLASRQRSLTREQLTEQLNCYLDLMRNVPYSTDSTVPSASASELID HALQMNKFEVEKDTIGDIIILPREQAVLMTYYRNNIAHMLVLPSLMAAIV TQHRHISRDVLMEHVNVLYPMLKAELFLRWDRDELPDVIDALANEMQ RQGLITLQDDELHINPAHSRTLQLLAAGARETLQRYAITFWLLSANPSI NRGTLEKESRTVAQRLSVLHGINAPEFFDKAVFSSLVLTLRDEGYISDS GDAEPAETMKVYQLLAELITSDVRLTIESATQGEGSGGGGSND**YPYDV PDYA**
PlsB-HaloTag	MSGWPRIYYKLLNLPLSILVKSKSIPADPAPELGLDTSRPIMYVLPYNSK ADLLTLRAQCLAHDLPDPLEPLEIDGTLLPRYVFIHGGPRVFTYYTPKE ESIKLFHDYLDLHRSNPNLDVQMVPVSVMFGRAPGREKGEVNPPLR MLNGVQKFFAVLWLGRDSFVRFSPSVSLRRMADEHGTDKTIAQKLAR VARMHFARQRLAAVGPRLPARQDLFNKLLASRAIAKAVEDEARSKKIS HEKAQQNAIALMEEIAANFSYEMIRLTDRILGFTWNRLYQGINVHNAER VRQLAHDGHELVYVPCHRSHMDYLLLSYVLYHQGLVPPHIAAGINLNF WPAGPIFRRLGAFFIRRTFKGNKLYSTVFREYLGELFSRGYSVEYFVE GGRSRTGRLLDPKTGTLSMTIQAMLRGGTRPITLIPIYIGYEHVMEVGT YAKELRGATKEKESLPQMLRGLSKLRNLGQGYVNFGEPMPLMTYLNQ HVPDWRESIDPIEAVRPAWLTPTVNNIAADLMVRINNAGAANAMNLCC

	TALLASRQRSLTREQLTEQLNCYLDLMRNVPYSTDSTVPSASASELID HALQMNKFEVEKDTIGDIIILPREQAVLMTYYRNNIAHMLVLPSLMAAIV TQHRHISRDVLMEHVNVLYPMLKAELFLRWDRDELPDVIDALANEMQ RQGLITLQDDELHINPAHSRTLQLLAAGARETLQRYAITFWLLSANPSI NRGTLEKESRTVAQRLSVLHGINAPEFFDKAVFSSLVLTLRDEGYISDS GDAEPAETMKVYQLLAELITSDVRLTIESATQGEGSGGGGSND**GSEIG** **TGFPFDPHYVEVLGERMHYVDVGPRDGTPVLFLHGNPTSSYVWRNII** **PHVAPTHRCIAPDLIGMGKSDKPDLGYFFDDHVRFMDAFIEALGLEE** **VVLVIHDWGSALGFHWAKRNPERVKGIAFMEFIRPIPTWDEWPEFAR** **ETFQAFRTTDVGRKLIIDQNVFIEGTLPMGVVRPLTEVEMDHYREPFL** **NPVDREPLWRFPNELPIAGEPANIVALVEEYMDWLHQSPVPKLLFWG** **TPGVLIPPAEAARLAKSLPNCKAVDIGPGLNLLQEDNPDLIGSEIARW** **LSTLEISG**

684